SECED 2023 Conference
Earthquake Engineering & Dynamics for a Sustainable Future
14-15 September 2023, Cambridge, UK

NUMERICAL MODELLING OF THE CYCLIC BEHAVIOUR OF RC COLUMNS GOVERNED BY FLEXURE AND FLEXURE-SHEAR

Ruoyu Hou[1], Cels Jonas[2], Marta Del Zoppo[3], Rossetto Tiziana[4]

Abstract: *This study focuses on the development of a numerical model for reinforced concrete (RC) columns under cyclic loading. A refined numerical model for representing the hysteretic behaviour of flexure and flexure-shear sensitive RC columns with poor seismic detailing is developed in OpenSees. The efficient modelling framework comprises flexure, bond slip, bars buckling and shear components to simulate the hysteretic behaviour of RC columns up to failure. To represent the shear component of its overall response, shear spring with limit state material and limit curve is adopted. The adopted model is able to accommodate three typical failure modes (i.e., flexural, flexure-shear and pure shear) and is validated with respect to quasi-static cyclic test results. The OpenSees model is seen to well reproduce the load-displacement relationships and backbone curves of tested RC columns. The results also suggest that developed numerical model can predict flexure-shear at expected drift level and is able to capture lateral-strength degradation induced by different failure modes.*

Introduction

Over the last few decades, columns characterized by poorly detailed transverse reinforcements have attracted wide attention in modern seismic risk assessment. Previous studies show that such these shear-sensitive columns are likely to experience premature shear failure that led to local shear damage and unexpected global failure sequences under earthquake scenario. Finite Element Model (FEM) has been recognized as the most robust and promising tool to accurately predict the cyclic hysteretic behaviour of RC member. However, to the author's best knowledge, predicting shear behaviour within inelastic range and post-failure rules are not well-understood up to date.

Numerical models for simulating nonlinear hysteretic behaviour of structural main components have been studied for decades. One of the mainstream branches in cyclic-loading modelling strategy is the lumped-plasticity model. The required nonlinearity of this typical framework is lying in the moment-curvature relationship assigned in preselected plastic hinges and require unique calibration on target specimen. While few study was focused on shear effects and even does, flexural-shear interaction is mostly excluded. For example, Pincheira et al. (1999) proposed a shear hinge model for RC columns in which shear and flexural behaviour are considered separately. Sung et al. (2005) incorporated shear behaviour into lumped plastic hinge model by transferring shear-rotation relationship into moment-curvature relationship. Another widely accepted approach is the discrete finite element model. Within which, flexural behaviour is represented by a limited number of interconnected fiber-based beam-column elements whereas a single shear spring is employed to account for shear responses (Filippou and Ambrisi, 1992; Berry and Eberhard, 2007). Most of these developed numerical macro models simplify the shear backbone curves into additional superimposed elastic translational behaviour and more than that, strength deterioration rules were not well-understood and well-defined.

[1] MSc Student, Department of Civil, Environmental and Geomatic Engineering, University College London, London, United Kingdom, Email: ucesrho@ucl.ac.uk

[2] PhD Candidate, Department of Civil, Environmental and Geomatic Engineering, University College London, London, United Kingdom

[3] Marie-Curie Research Fellow, Environmental and Geomatic Engineering, University College London, London, United Kingdom

[4] Professor, Department of Civil, Environmental and Geomatic Engineering, University College London, London, United Kingdom

Lucchini et al. (2022) observed that shear deflection can still be significant even if the column is not governed by shear failure. With the support data from a recent experimental campaign performed by Lucchini et al. (2022), a numerical model has been developed in OpenSees to predict nonlinear cyclic behaviour of RC columns subject to 3 typical failure modes, namely flexural-critical (FC), flexural-shear-critical (FSC) and shear-critical (SC). The shear behaviour of columns is simulated through the limit state material available in OpenSees. The adopted numerical model has been validated on 6 experimental tests from literature and results are reported in the paper.

Experimental database

A total of 6 RC columns classified by 2 configuration types tested in the experimental campaign performed by Lucchini et al. (2022) are selected for this study. The experimental setup as well as its comprised apparatuses are elaborated in Lucchini et al. (2022). Specimens being selected for this study are representative of existing columns with poor amount of transverse reinforcement in a low-rise four-story building in southern Europe. Figure 1 provides a schematic view of geometry and reinforcing details of tested columns. The lateral force is applied at a distance of 1.50 m from the top surface of foundation block. All the selected columns are characterised by a uniform 300 $\times$300 mm square cross section including a 25-mm thickness concrete cover. Each section is comprised by four continuous 16-mm longitudinal reinforcements and 2-legged stirrups of 6-mm diameter anchored by 90 degrees bends. While the spacing of stirrups are varied in two classified columns with 150 mm in left denoted by L (low) and 250mm in right denoted by VL (very low). The displayed block foundation which has five additional stirrups of 10 mm diameter and 20 mm thickness of concrete cover in each direction is anchored into a stiff steel socket to provide fixed constraints and reproduce an idealized cantilever scheme.

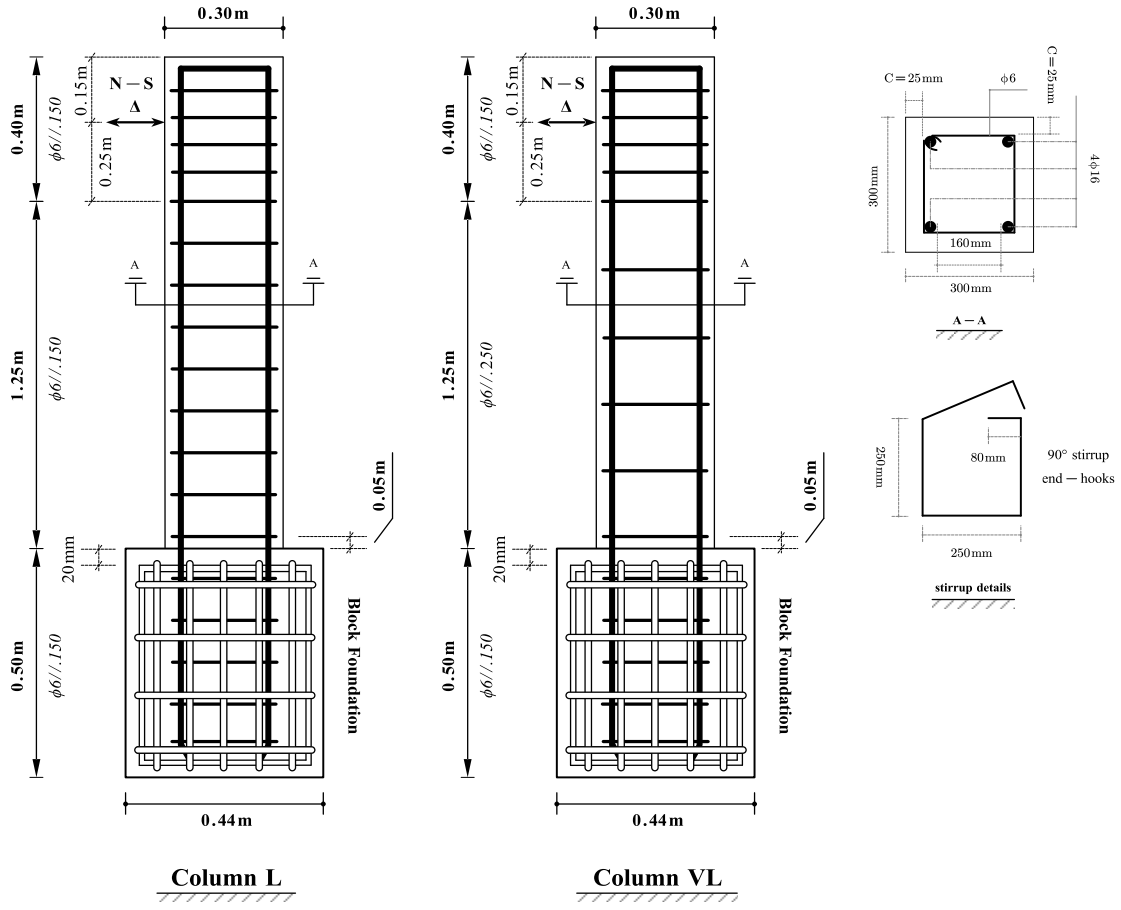

Figure 1. Specimen geometry and reinforcing details

Table 1 thoroughly summarizes their mean material properties, geometrical characteristics and applied loading protocols. It is worthy to mention that the mean compressive strength of concrete

is reported in terms of standard concrete cylinder strength on 2:1 sample with 15-mm diameter. In the specimens naming, suffix letters L denotes a column with low amount of reinforcement with transverse reinforcement ratio of 0.126% while VL represents a lower value of 0.075%. Two axial load levels including 150 kN and 450 kN are selected aiming to investigate the axial load effect upon their failure modes. They are accordingly distinguished by labelling the numbers 10 and 20 respectively which are essentially referring to their corresponding approximate axial load ratios in percentage.

Specimen (Loading pattern)	**Shear reinforcement ratio**	**Axial load**	**Concrete compressive strength**	**Steel yield strength**	**Steel ultimate strength**	**Stirrup yield strength**	**Stirrup ultimate strength**
	%	*kN*	*MPa*	*MPa*	*MPa*	*MPa*	*MPa*
L10 (UCS)	0.126	150	21.1	433.6	584.6	459.7	565.5
L20 (UCS+UCA)	0.126	450	31.0	464.7	585.7	459.7	565.5
VL10 (UCS+UCA)	0.075	150	22.4	433.6	584.6	459.7	565.5
VL20 (UCS)	0.075	450	23.7	464.7	584.6	459.7	565.5

Table 1. Description of tested specimens

This experimental test involved simultaneous application of vertical and horizontal loading. Lateral Loading path is a uniaxial cyclic displacement time history in N-S direction where W-E direction is completely restrained. It can be furtherly classified as two categories dependent on the symmetry of displacement pattern in pull and push direction, namely uniaxial cyclic symmetric (UCS) and uniaxial cyclic asymmetrical (UCA). The displacement history requires the member to displace to a target drift three times (two times for UCA) before moving to a next cycle with higher value of displacement. Meanwhile, the axial load is keeping constant where the small rotation caused by angle between sliding plate and vertical actuator is post-processed after reading the data. The maximum imposed displacement is set as a value of 100 mm (6.5% drift). The test has been stopped when the maximum displacement was reached.

Basic framework of adopted numerical model

In this study, general framework for simulating hysteresis behaviour of most three common types of cantilever column classified by global failure modes is developed. Generally speaking, it can be decomposed into two independent parts that account for flexure deformation and shear deformation respectively. Nevertheless, the relevant failure types should be determined prior to the modelling process as each of them yield different ductility levels.

Localization problem in OpenSees Modelling

Strain localization as frequently occurred in those elements comprised from softening section with high nonlinearities demand will directly affect the performance of assembled model. In this study, a different approach that using displacement-based element (DBE) is employed to deal with the localization problem. Stress and strain in DBEs are computed from displacement field at only structural level. Therefore, instead of localizing at one integration point, the curvature demand will allocate to a single element which make localization issue less pronounced (Coleman and Spacone, 2001). However, the stiffness-based formulation in DBE makes it inherently rigid and ends in stiffer responses compared to real one. But so long as sufficient elements are provided to represent the whole length of member, the peak response will decrease and approach to real demand without post-processing. While this kind of mesh-dependent nature of response is not cumbersome to regularize and can either use trial-and-error or simply match the first element with empirical plastic hinge length.

Numerical model for flexural behaviour

The flexural component of the overall deflection is modelled by 6 DBEs to ensure the objective response and meanwhile avoid localization problem. The fiber-based technique is employed to the section model where the required nonlinearity is attributed to its assembled material model. Each member section is subdivided into three parts that represent the cover concrete, confined concrete, and steel bars. Each part is assigned by an appropriate constitutive material law via fibers that lie within the corresponding area. A unified material model incorporating effective

lateral confining stress from arching action between two neighbouring hoops proposed by Mander et al. (1988) is used to define the required parameters in "*Concrete04*" material model for confined concrete. The unconfined concrete fibers are represented by the same material model within which comprised properties are determined from standard cubic tests. Similarly, steel fibers are assigned by either "*Hysteretic Material*" Model or "*Steel 02*" constitutive law relationship. However, the result will only display the model which gives the best approximation over force-displacement relationship. To prevent steel strain hardening response from dominating the post-peak behaviour, the ultimate strain of steel is bidirectionally limited by 5% via "*MinMax Material*". Table 2 & 3 summarize the parameters as aforementioned where the relevant references are also included.

Fiber	**Model**		f_c'	ε_0	ε_u	E_c	f_{ct}	E_t	ε_t
			MPa	-	-	*MPa*	*MPa*	*MPa*	-
Cover concrete	*Concrete 04*	**Ref**	concrete cubic test				EN 1992-1-1 T3.1	-	-
		Val	-	0.002	0.004	-	$0.3 \times (f_c' - 8)^{2/3}$	E_c	f_{ct}/E_t
Core concrete	*Concrete 04*	**Ref**	J.B.Mander (1988)				EN 1992-1-1 T3.1	-	-
		Val	-	-	-	-	$0.3 \times (f_c' - 8)^{2/3}$	E_c	f_{ct}/E_t

Table 2. Concrete material model

Fiber	**Model**		b_s	E_s	e_{1p}	s_{1p}	e_{2p}	s_{2p}	ε_{max}	$PinchX$	$PinchY$	$beta$
			-	*MPa*	*MPa*	-	*MPa*	-	%	-	-	-
Steel	*Hysteretic*	**Ref**	empirical		uniaxial tensile test				empirical			
		Val	0.005	21e^4	-	-	-	-	5	0.4	0.6	0.4
Fiber	**Model**		b	E_s	$cR1$		$cR2$		R_0		f_y	
			-	*MPa*	-		-		-		*MPa*	
Steel	*Steel02*	**Ref**	empirical		empirical				calibrated		tensile test	
		Val	-	21e^4	0.925		0.15		-		-	

Table 3. Steel material model

Flexural deformation exerted by column should include both the deformation due to the curvature over the column and concentrated rotation caused by bar slip. Matter of fact, the anchorage slippage of longitudinal rebar known as strain penetration is likely to affect the cyclic behaviour of RC column by inducing fixed-end rotation. Hence, to account for the additional contribution on overall flexibility, a rotational spring at base end is included by means of zero-length element in this study. For the sake of simplicity, the plain bar slip is excluded in the adopted model and a linear elastic material is assigned to the rotational degree of freedom. The rotational stiffness of bar-slip spring is calculated according to the work contributed by Elwood & Eberhard (2009). Mathematically, it is given by the following equation:

$$K_{slip} = \frac{8u}{d_b f_s} \frac{M_{0.004}}{\phi_y} = \frac{8u}{d_b f_s} EI_{flex} \tag{1}$$

Where u is the constant/average bond stress along the embedded bars and we can simply take as $0.8\sqrt{f_c'}$ which is consistent with the calibration data in their study. EI_{flex} is the effective flexural stiffness of column. This can be obtained by building a sectional analysis framework in OpenSees in which using a zero-length section element to extract the relevant parameters when the concrete cover strain reaches concrete crushing stain (0.004). To assure the stability of this framework, all the degrees of freedom require to be restrained except the translational and rotational directions of the top node.

Numerical model for shear behaviour

Classical shear modelling approach that considers shear response by means of adding an empirical shear response backbone model is simplistic but neglect the shear-flexural interaction. Such shear degrading is only captured by the estimated shear strength, and this might stand up for a short squat whose failure model is completely brittle, for those columns that shear strength decay with ductility development or "strong shear weak bending", this may give a unobjective reflection of its deteriorating behaviour. Plus, the post-failure response is not well-understood from this approach due to the lack of nonphysical damage definition. To overcome these problems, OpenSees platform introduced "Limit State Material (LM)" on the basis of work from Elwood (2004). This model defines a limit surface derived from an empirical drift capacity model (Elwood and Moehle, 2005a, 2005b) and triggers a change in the predefined hysteretic behaviour once the load-deformation behaviour of column intersects the limit curve. As depicted in Figure 2, a

well-defined shifted limit curve can be served for a general purpose. Such this mentality provides the possibility that any failure mode related to a capacity model and whose post-failure behaviour is featured by a sudden change in behaviour triggered by a certain limit level can be modelled via this approach. As shear failure modes can be described by different ductility level, it lays the groundwork for the proposals.

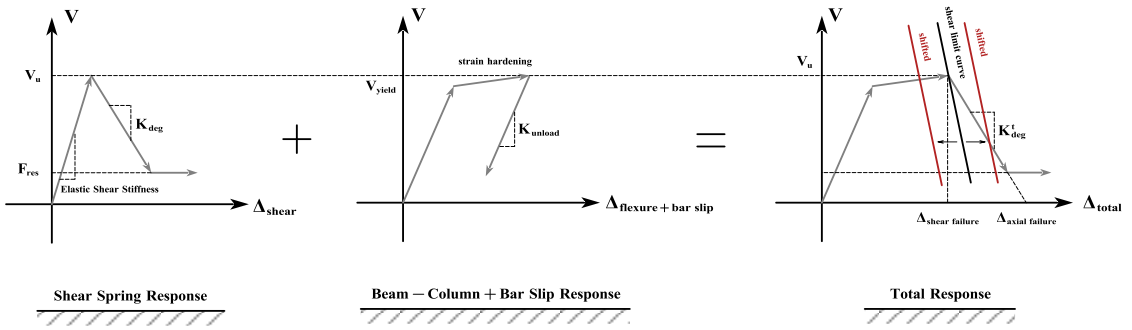

Figure 2. Uniaxial limit state material model (Elwood 2004)

Within this framework, flexural behaviour is assumed to be only and entirely captured by force-beam element whereas shear component is concentrated at shear spring. Flexure-shear interaction is arranged at element level in a way of a monitoring process over the current force and displacement state on column at each converged step. After shear failure is detected by the limit curve, an additional deformation result in both strength degradation and shear deformation increment. It's also worthwhile to mention that flexure-shear coupling at element level can also be enhanced in a displacement-based approach. Limit curves come from empirical displacement-based model have already incorporated the influence of flexural deformation into the model if it is well-selected.

In the adopted model, pre-failure shear backbone requires to be clarified as for establishing hysteretic rules before encountering the peak response or displacement at predicted failure point. In this study, shear component of total deflection will be explained in accordance with the elastic theory:

$$\Delta_{shear} = k\frac{VL}{GA_g} = k\frac{2(1+\nu)}{E_c A_g}VL \tag{2}$$

Where k is a shape factor for cross section and can take 1.0 for rectangular section and 4/3 for circular section; ν is the Poisson ratio of concrete; E_c is the young modulus of concrete; A_g is the gross cross-sectional area of column; L is the entire length of column; V is the transverse shear force. It is worthwhile to highlight that shear constitutive law requires to be defined in an increasing order so that they all lay on the same line.

Numerical model for FC column

The experimental observation on L10 and VL10 specimens under symmetrical cyclic loading suggest that longitudinal rebars buckled parallel to the face of the columns at middle stage whereas transverse hoops have little effect. FC columns characterized by large-size longitudinal bars and lower strength concrete and poor transverse reinforcement ratio are prone to bar buckling. Bar buckling not only reduce the expected ductility and deformation capacity, but also give rise to both strength and stiffness degradation. Instead of involving too much hysteretic details by incorporating buckling behaviour into the constitutive law of steel material model, accurately predicting the onset of bar buckling and identifying post-buckling strength or stiffness will be more of interest in this study. To this end, Berry & Eberhard (2005) derived an empirical equation to approximate the drift ratio of the onset of bar buckling based on calibration of 104 tested RC columns:

$$\frac{\Delta_{bb}}{L}(\%) = 3.25(1+k_{e\_bb}\rho_{eff}\frac{d_b}{D})(1-\frac{P}{A_g f_c'})(1+\frac{L_c}{10D}) \tag{3}$$

Where Δ_{bb} is the displacement at bar buckling failure; k_{e_bb} is the transverse reinforcement coefficient which takes 40 for rectangular-reinforced columns and 50 for spiral-reinforced and 0 if

s/d_b exceeding 6.0; d_b is the diameter of longitudinal reinforcement steel; $\rho_{eff} = \rho_s f_{yt}/f_c'$ is the effective confinement ratio and ρ_s is the volumetric transverse reinforcement ratio (volume of hoop to volume of core); D is the column depth; L_c is the distance between the column base and the contraflexure point.

Notice that the default limit curve is designed for a shear-critical column as mentioned by Elwood (2004). To substitute this "buckling limit curve", the original one requires to be shifted to the predicted buckling point by using "delta" function which is the last input parameter in the Limit Curve command:

$$delta_F = \Delta_{bb} / L - \Delta_s / L \tag{4}$$

Where Δ_s is the displacement at shear failure which ought to be evaluated according to the drift capacity model in Elwood and Moehle (2005b). The estimated displacement at collapse can be empirically assumed as twice over buckling displacement (Liu et al., 2015). Consequently, based on the linear feature in post-peak backbone curve illustrated in Figure 2, degrading slope of total response can be evaluated as:

$$K_{\text{deg}}^{t} = -\frac{V_u}{\Delta_{collapse} - \Delta_{buckling}} = -\frac{V_u}{2\Delta_{bb} - \Delta_{bb}} = -\frac{V_u}{\Delta_{bb}} \tag{5}$$

Where V_u is the shear strength limit and is approximated from the ductility-dependent degrading shear strength model established by Sezen and Moehle (2004) for this study. As beam-column element and shear spring are placed in series, the flexibility (degrading stiffness) of shear spring can be reversely derived as follow:

$$K_{\text{deg}}^{shear} = \left(\frac{1}{K_{\text{deg}}^{t}} - \frac{1}{K_{unload}}\right)^{-1} = \left(-\frac{\Delta_{bb}}{V_u} - \frac{L^3}{3EI_{flex}}\right)^{-1} \tag{6}$$

Numerical model for FSC column

FSC Column has slightly higher shear strength than flexural strength which allows them to yield in flexure prior to shear failure. Compared with the FC column, they tend to exhibit a relatively lower ductility and larger smeared diagonal shear cracks in the hinge region. Shear strength deterioration occur after the plasticity in hinge region develop to a fully extent. From our experimental test observation, a quicker and larger shear strength degradation is found to be more pronounced in these columns equipped with low shear reinforcement under higher axial load level. This suggest that local shear damage becomes the main issue in post-peak stage and dominates the strength-degrading cyclic behaviour. Previous adopted model for FC column cannot be applicable in this case and require a unique analytical model.

Given the key roles in displacement-based assessment in modern seismic design, the general framework for numerical model that simulate FSC column's hysteretic behaviour is still built upon LM model. To the author's best knowledge, currently there hasn't been a robust drift model to predict the onset of FS failure. However, this can be overcome by adopting a hinge rotation model and a simple transformation by relating end rotation to tip displacement. Ghannoum (2007) observed that shear failure in FSC column only happened after the plastic hinge deteriorates sufficiently and with 56 columns failed in flexural-shear failure test data, an empirical shear failure initiation model was proposed by relating shear strength degradation to column end rotation. Mathematically, it is given by the following equation:

$$\theta_{hinge} = 0.044 - 0.017\frac{s}{d} - 0.021\frac{P}{A_g f_c'} - 0.002\frac{v}{\sqrt{f_c'}} \geq 0.009 \tag{7}$$

Where v is the nominal shear stress and is recommended to be evaluated by V_u/A_g. In a simple fixed-free boundary condition without any additional framed imposed constraint, the relevant tip displacement can be approximately calculated as below:

$$\Delta_{FS} = L \cdot \tan\left(\theta_{hinge} \cdot \frac{180°}{\pi}\right) \tag{8}$$

Where Δ_{FS} is the tip displacement at flexural-shear failure. Hence, to activate the flexural-shear failure limit surface, original shear limit curve is required to be regulated by drifting it in a value of:

$$delta_{FS} = \Delta_{FS} / L - \Delta_s / L \tag{9}$$

To be consistent with calibrated data, the overall strength degrading slope will be subtracted from the same testing data. A mean value of -2500N/mm and a minor value of -400 N/mm and a maximum value of -12000 N/mm were summarized in LeBorgne and Ghannoum (2010). The degrading stiffness of shear spring can be calculated in the same way as aforementioned, but the assignment of total post-peak degrading slope requires engineering judgement. According to the experimental observation in this campaign, at given drift demand, post-peak degrading slope caused by cyclic loading is increasing from UCA to UCS. As a result, the ductility of same column is inversely seen reduced from UCA to UCS. Those FSCs subjected to UCS loading pattern are more closed to the mean value whereas reported minor value is more appropriate to be assigned in UCA loading scenario.

Numerical model for SC column

A pure shear failure is often followed by axial failure due to the primary diagonal shear crack which means a shear critical column is vulnerable to shear-axial failure. Differentiating from any other shear failure mode, SC columns usually experience shear damage prior to yielding which indicates that the overall capacity is limited by the maximum shear strength. For more slender columns, shear degradation is still activated by the overall lateral deformation. A drift capacity model derived from a data base of 50 shear-critical RC columns for the purpose of shear failure initiation was proposed by Elwood and Moehle (2005b):

$$\frac{\Delta_s}{L} = \frac{3}{100} + 4\rho'' - \frac{1}{40}\frac{v}{\sqrt{f_c'}} - \frac{1}{40}\frac{P}{A_g f_c'} \geq \frac{1}{100}(MPa) \tag{10}$$

Where ρ'' is the shear reinforcement ratio given by A_{st}/bs. As this equation is the default shear limit curve assigned in LM model which means there is no need to shift it. This model is always combined with another shear friction model (Elwood and Moehle, 2005a) meant for determining the onset of axial failure and degrading stiffness in a typical SC column within the calibrated range:

$$\frac{\Delta_a}{L} = \frac{4}{100}\frac{1+(\tan\theta)^2}{\tan\theta + P(s / A_{st} f_{yt} d_c \tan\theta)}(MPa) \tag{11}$$

Where $\theta = 65°$ is the critical crack angle from the horizontal; d_c is the depth of column core from centreline to centreline of the ties; Δ_a is the tip displacement at axial failure. Axial failure occurs when conserved shear strength degraded to approximately zero (Nakamura and Yoshimura, 2002). Therefore, the corresponding post-peak degrading slope is determined as follow:

$$K_{\text{deg}}^{t} = -\frac{V_u}{\Delta_a - \Delta_s} \tag{12}$$

Summary of adopted numerical model

For the sake of brevity, the composition of adopted general framework is illustrated in Figure 3. Beam-column element modelled by 6 DBEs is placed in series with a zero-length element whose first degree of freedom (DOF) is a representative shear spring while bar slip component is embedded into DOF 6. Axial limit curve is excluded in suggested modelling strategy since the flexure and flexure-shear failure modes are the focus of this study. All degrees of freedom at base end are fixed whereas those at loaded end are released to free to replicate experimental context. To make sure the convergence and stability of adopted framework, nonlinear quasi-static analysis is conducted under an adaptive solution algorithm package including Newton-Raphson, Modified Newton-Raphson, Broyden and Newton-Raphson with Line Search checked against a fixed tolerance threshold of 1.0e-8. In the following, validation work will be conducted for two of adopted models by means of 6 columns as they either failed in flexure (F) or flexure-shear (F-S) failure. While adopted framework for SC column will not be included in this study due to the limitation of the experimental data set.

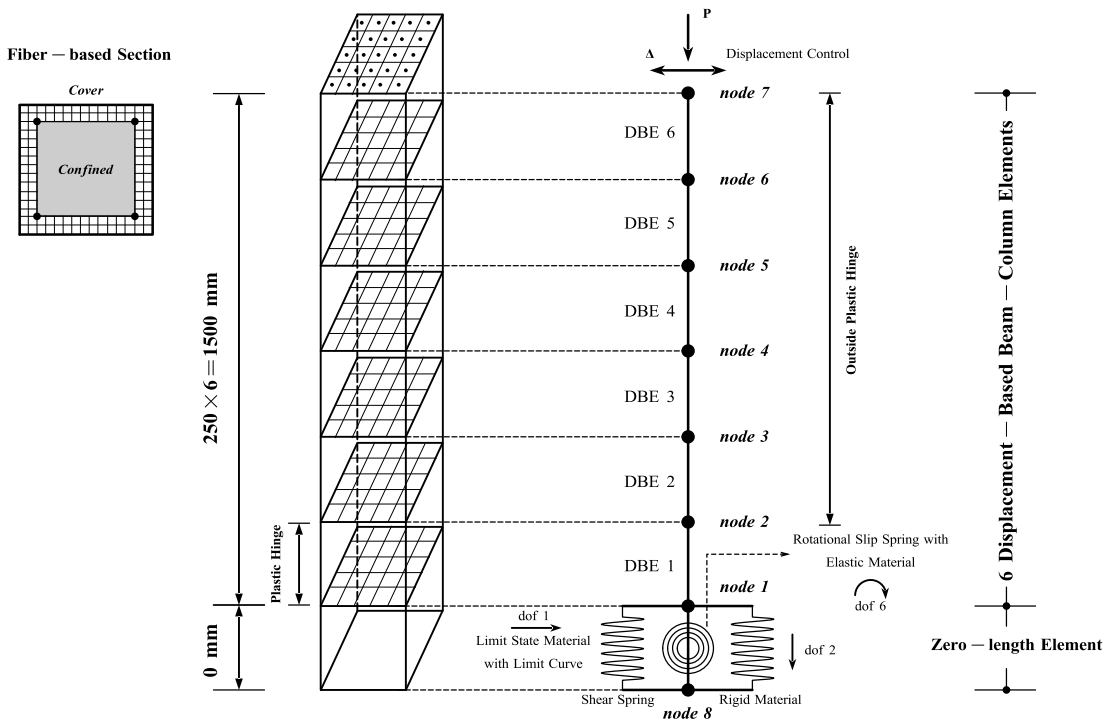

Figure 3. Schematic of composition of adopted numerical model

Validation of adopted numerical model

The implementation of adopted model in the selected 6 columns along with the responding experimental results are displayed from Figure 4 to 6. Blue dot dash line marked in each figure depicts each specimen unique failure surface or limit surface as defined in advance. BLM refers to the limit curve associated with buckling failure whereas SLM denotes the limit curve that deal with flexure-shear failure. In terms of the hysteretic-loop comparisons, adopted model visually exhibits a fairly good agreement with experimental test results. Numerically, derived model gives accurate prediction over maximum shear strength, overall hysteretic dissipative energy, and degrading slope of applied columns. As for adopted strategy for FC column, the buckling failure points are found to be activated at accurate time steps. This also imply the decent predictive performance of adopted drift capacity model. The post-failure degrading slope is generally consistent with experimental post-peak backbone curve although the residual strength more or less has a certain percentage error.

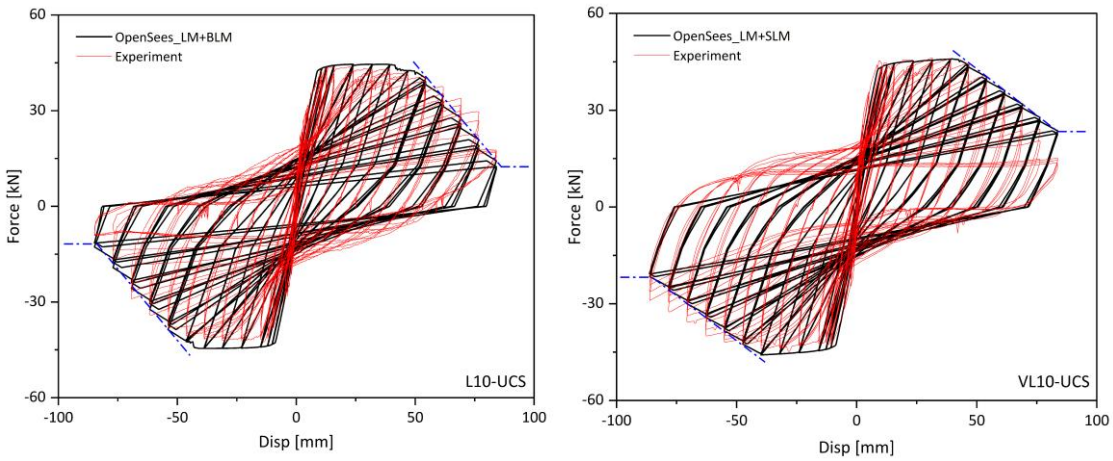

Figure 4. Hysteresis curve comparison for specimens subjected to UCS failed in F

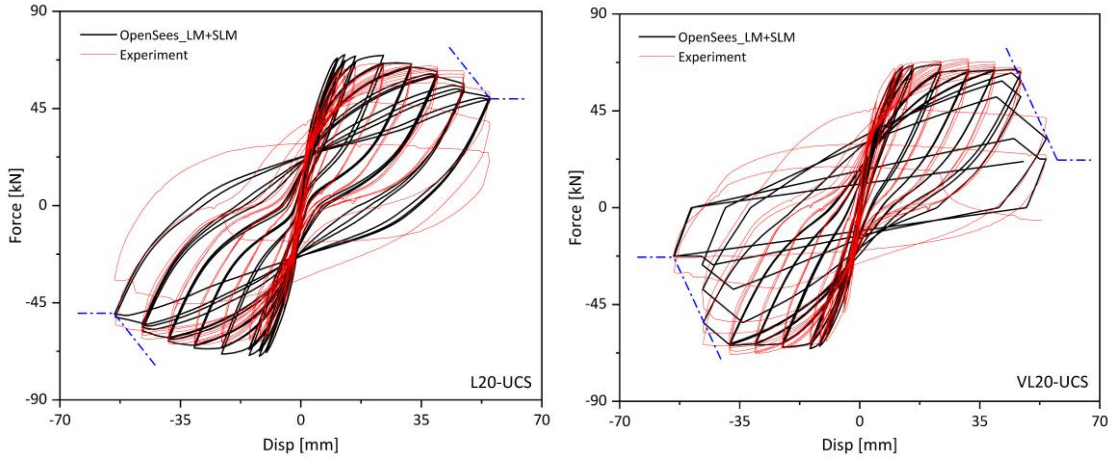

Figure 5. Hysteresis curve comparison for specimens subjected to UCS failed in F-S

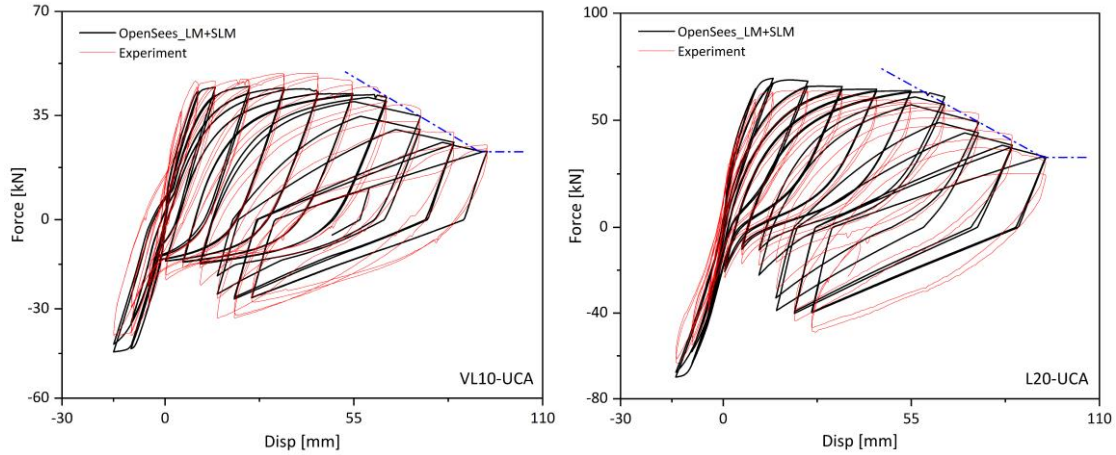

Figure 6. Hysteresis curve comparison for specimens subjected to UCA failed in F-S

With respect to verified FSC columns, flexural-shear failure was detected at precise displacement level in all cases. Figure 5 and Figure 6 show that, FE model that employs *Steel02* can simulate the nonlinear response more decently before the post-failure behaviour being triggered. In specimen L20 subjected to UCS loading pattern, the strength degradation is not obvious as others. This is owing to the observation that the flexural-shear failure point in this case is detected at a displacement level of around 52 mm which is quite closed to the terminating point of loading. It's important to highlight that less amount of transverse reinforcement led to early shear degradation and reduction of ductility. And this rule is found to be explained by the adopted model thoroughly.

It is also interesting to observe that those columns featured by a lower concrete strength appear to yield slightly higher initial stiffness. This may imply that concrete model employed in this study for estimating modulus of elasticity proposed by Mander et al. (1988) is not reliable for low-strength concrete. Matter of a fact, it was being found a significant difference between the EC2 recommendation and adopted model result over the derived value. However, adopted model employs a simple idealized cantilever scheme without considering the realistic material and reinforcement properties of block foundation which means that theoretically ought to overestimate the initial response slope. But since we incorporate the bar slip behaviour into the model and as a result, the overall flexibility is somewhat being redeemed in this way.

Conclusions

This study was conducted to develop a modelling strategy able to simulate the cyclic behaviour of existing RC columns. The developed OpenSees model produces accurate simulations of force-displacement relationship derived from 6 tested columns which failed in flexure and flexure-shear modes. The adopted numerical models are verified to be capable of detecting the buckling and

the flexure-shear interaction at expected displacement levels owing to the robust performance of adopted empirical drift capacity models. Future studies will look at the validation of the adopted models on shear-critical RC columns and at the upgrade to 3D models that are able to simulate bidirectional loading protocols.

References

Berry, M.P. and Eberhard, M.O. (2005) 'Practical Performance Model for Bar Buckling', *Journal of Structural Engineering*, 131(7). Available at: https://doi.org/10.1061/(asce)0733-9445(2005)131:7(1060).

Berry, M.P. and Eberhard, M.O. (2007) *Performance Modeling Strategies for Modern Reinforced Concrete Bridge Columns*.

Coleman, J. and Spacone, E. (2001) 'Localization Issues in Force-Based Frame Elements', *Journal of Structural Engineering*, 127(11). Available at: https://doi.org/10.1061/(asce)0733-9445(2001)127:11(1257).

Elwood, K.J. (2004) 'Modelling failures in existing reinforced concrete columns', *Canadian Journal of Civil Engineering*, 31(5). Available at: https://doi.org/10.1139/L04-040.

Elwood, K.J. and Eberhard, M.O. (2009) 'Effective stiffness of reinforced concrete columns', *ACI Structural Journal*, 106(4). Available at: https://doi.org/10.14359/56613.

Elwood, K.J. and Moehle, J.P. (2005a) 'Axial capacity model for shear-damaged columns', *ACI Structural Journal*, 102(4). Available at: https://doi.org/10.14359/14562.

Elwood, K.J. and Moehle, J.P. (2005b) 'Drift capacity of reinforced concrete columns with light transverse reinforcement', *Earthquake Spectra*, 21(1). Available at: https://doi.org/10.1193/1.1849774.

Filippou, F.C. and Ambrisi, A.D.' (1992) *NONLINEAR STATIC AND DYNAMIC ANALYSIS OF REINFORCED CONCRETE SUBASSEMBLAGES*.

Ghannoum, W. (2007) 'Experimental and analytical dynamic collapse study of a reinforced concrete frame with light transverse reinforcement', *PhD Thesis* [Preprint].

LeBorgne, M.R. and Ghannoum, W.M. (2010) 'Modeling the degrading shear behavior of reinforced concrete columns to collapse', in *9th US National and 10th Canadian Conference on Earthquake Engineering 2010, Including Papers from the 4th International Tsunami Symposium*.

Liu, K.Y., Witarto, W. and Chang, K.C. (2015) 'Composed analytical models for seismic assessment of reinforced concrete bridge columns', *Earthquake Engineering and Structural Dynamics*, 44(2). Available at: https://doi.org/10.1002/eqe.2470.

Lucchini, A. *et al.* (2022) 'Load Path Effect on the Response of Slender Lightly Reinforced Square RC Columns under Biaxial Bending', *Journal of Structural Engineering*, 148(3). Available at: https://doi.org/10.1061/(asce)st.1943-541x.0003231.

Mander, J.B., Priestley, M.J.N. and Park, R. (1988) 'Theoretical Stress‐Strain Model for Confined Concrete', *Journal of Structural Engineering*, 114(8). Available at: https://doi.org/10.1061/(asce)0733-9445(1988)114:8(1804).

Nakamura, T. and Yoshimura, M. (2002) 'Gravity Load Collapse of Reinforced Concrete Columns with Brittle Failure Modes', *Journal of Asian Architecture and Building Engineering*, 1(1). Available at: https://doi.org/10.3130/jaabe.1.21.

Pincheira, J.A., Dotiwala, F.S. and D'Souza, J.T. (1999) 'Seismic analysis of older reinforced concrete columns', *Earthquake Spectra*, 15(2). Available at: https://doi.org/10.1193/1.1586040.

Sezen, H. and Moehle, J.P. (2004) 'Shear Strength Model for Lightly Reinforced Concrete Columns', *Journal of Structural Engineering*, 130(11). Available at: https://doi.org/10.1061/(asce)0733-9445(2004)130:11(1692).

Sung, Y.C. *et al.* (2005) 'A study on pushover analyses of reinforced concrete columns', *Structural Engineering and Mechanics*, 21(1), pp. 35–52. Available at: https://doi.org/10.12989/sem.2005.21.1.035.